12
Magnetisation deficit anomalies

C.A. Foss

ABSTRACT

Sharp magnetic anomalies most commonly arise due to localised strong ('anomalous') magnetisation in contrast to surrounding weaker magnetisation. However, less commonly, magnetic field anomalies are due to absent or weak magnetisation surrounded by stronger magnetisation. I present two studies to illustrate inversion of these 'deficit' magnetisation anomalies. The first study is of the normally magnetised Kalkarindji basalts in the Northern Territory. There is an extensive magnetic high over a wide sheet of basalt with sharp negative anomalies at what appear to be fracture intersections in the sheet. I interpret these magnetic anomalies as due to destruction of magnetisation where the sheet has been altered by heated waters escaping through those fracture intersections from the underlying Beetaloo Basin. Inversion of these anomalies on the assumption that magnetisation is completely destroyed provides estimates of the magnetisation of the surrounding sheet. In the second example I interpret an elliptic region of approximately 8 km diameter of low and smoothly varying magnetic field values north of Ceduna in South Australia as due to a non-magnetic or weakly magnetic granite intruded into surrounding more strongly magnetised basement. Modelling the granite against a nominated surrounding zero magnetisation recovers a magnetisation estimate that can be reversed in direction and assigned to the basement rocks. In this example the magnetisation of the surrounding basement is variable in strength and to obtain a magnetisation estimate from the contrast against the granite I have excised local high-amplitude anomalies. Independent inversion of some of those anomalies returns magnetisation estimates consistent with the basement magnetisation direction inferred from the granite anomaly inversion. This suggests that although the basement magnetisations are highly variable in strength, they are commonly directed. For both these studies the magnetisation contrasts are rotated from the local geomagnetic field directions, suggesting that remanence contributes to those magnetisations.

12.1 INTRODUCTION

Magnetic field modelling and inversion results are almost invariably discussed in terms of absolute magnetisations (or magnetic susceptibility values) whereas gravity modelling and inversion are commonly discussed in terms of density contrasts. In both cases measured variations in the gravity or magnetic field arise due to contrasts in physical properties. Lateral variations in subsurface density are rarely more than 10% of the total density. However, magnetisation contrasts are commonly a much higher proportion of total magnetisation,

with one magnetisation intensity that is inconsequential compared to the other. Another factor discouraging reference to contrasts in magnetic field modelling and inversion are that magnetisation contrasts are vectors rather than scalars and it is more challenging to assign meaning to vector contrasts than to scalar contrasts.

Voxel inversions of magnetic fields are increasingly being used to supposedly map continuous distribution of magnetisation in the subsurface. It is essential to realise that the magnetic field signal only provides information about magnetisation contrasts and that absolute magnetisations cannot be determined by inverse methods. The most reliable inversion results are obtained by focus on only the most discrete field variations (referred to throughout this book as 'sweet-spots') on the assumption that these magnetisations are in contrast with much weaker magnetisation.

One context for which magnetisation contrasts are sometimes discussed is the question of whether a negative amplitude TMI anomaly (in moderate to steep inclination fields) is due to reverse remanent magnetisation or a magnetic susceptibility lower than the surrounding material. This ambiguity is best resolved by searching beyond the immediate anomaly for any other marginal anomalies due to contrasts against what might be a strong enclosing magnetisation. For weak or diffuse anomalies this test is less diagnostic. Figure 12.1 illustrates a synthetic magnetic profile over both a local reverse magnetisation within a non-magnetic background (plotted in blue) and a magnetisation deficit (a hole) in a normal magnetisation background (plotted in red). The local anomalies themselves are almost identical, and the only chance of discriminating between their sources would be through recognition that the broader magnetisation (with a hole in it) contributes to the background field. Inversion of the magnetic field variation caused by a hole gives an apparent magnetisation direction opposite to that of the surrounding magnetisation, with inclination of opposite polarity and declination rotated by 180°. The two interpretations of a discrete reverse magnetisation or a cavity in magnetisation are end-case models in which one component is assumed to have zero strength relative to the other. Without this assumption, estimation of either magnetisation is highly non-unique. Without multiple constraints, voxel inversions in which the magnetisation of each element of the ground is assigned an absolute magnetisation intensity and/or direction are indefensible.

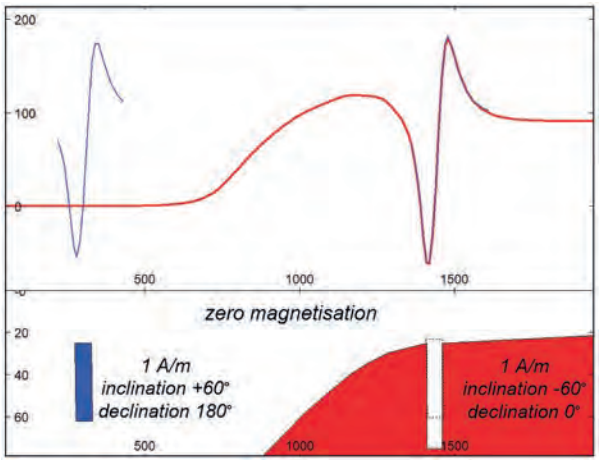

Fig. 12.1. Equivalent anomalies produced by a body with reverse magnetisation (in blue) and a hole in a body of normal magnetisation (in red).

If the ground beneath a well measured magnetic field consists of only two completely induced magnetisations of different strength (a single contrast in magnetic susceptibility) there should be no bias towards estimation of the directions of those magnetisations. However, many complex distributions of variously directed magnetisations can be misrepresented as suitably distributed zones of high and low magnetic susceptibility in a background of intermediate susceptibility. Figures 12.2A and 12.2D show two TMI anomalies of very different pattern in a −60° inclination field due to magnetisations of declination 30°, inclination −45° and declination 300°, inclination +15° respectively. In this relatively steep southern inclination geomagnetic field the contrast in declination of magnetisation can be estimated from the trough to peak azimuth and the contrast in inclination can be estimated from the peak and trough amplitude ratio (see Chapter 10). However, it is also possible to emulate these anomalies with only induced magnetisations. In this high-inclination field, TMI field variations are predominantly positive over high magnetic susceptibilities and negative (weaker than surrounding values) over low magnetic susceptibilities. The anomaly peaks and troughs due to the two single magnetisations as imaged in Figs 12.2A and 12.2D can be approximately matched with a distribution of magnetisation consisting of higher susceptibility towards the anomaly peak and lower susceptibility towards the trough as shown in the perspective views of Figs 12.2C and 12.2F. A simple magnetisation such as the single magnetisation dipole models used to generate the anomalies in Figs 12.2A and 12.2D can always be

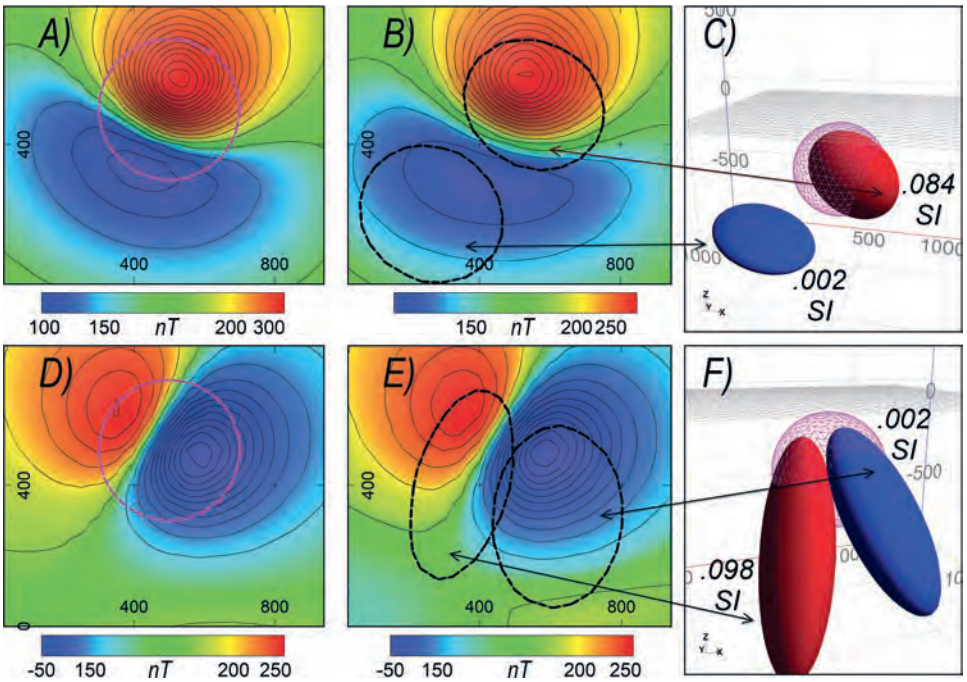

Fig. 12.2. TMI anomalies in a −60°inclination field due to remanent magnetisations: A) and D) and almost identical anomalies: B) and E) due to pairs of low and high susceptibility magnetisations. The remanent magnetisations are isolated and the induced magnetisations are in a background of 0.05 SI. C) and F) show the model perspectives: magenta – remanently magnetised sphere, red and blue – high and low susceptibility ellipsoids.

matched by more complex magnetisations given sufficient degrees of freedom. Conversely, few magnetisations due to complex distributions of high and low magnetic susceptibility can be closely matched by an alternative model of a single, compact magnetisation. Although the anomalies shown in Fig. 12.2 can be generated by either a simple single magnetisation model or a model of both high and low magnetic susceptibility, should such an anomaly be encountered in measured data, in the absence of any alternative information the more justified interpretation is that it is due to a single magnetisation. Complexity should only be added to magnetisation models as required. Note that transforms such as total gradient (TG) or the normalised source strength (NSS) sometimes applied to highlight the location of magnetisation, primarily highlight location of curvature in the magnetic field. If the TMI fields due to the alternative magnetisation models in Fig. 12.2 are identical then any enhancement transforms of those fields are also identical. Where there are minor differences between the alternative model fields the transforms at best emphasise those differences. Enhancements may assist in discriminating between models but they rarely provide diagnostic discrimination where that was not evident in the primary data.

12.2 MAGNETISATION DESTRUCTION ANOMALIES OVER THE KALKARINDJI BASALTS IN THE NORTHERN TERRITORY

Figure 12.3 shows the location of the study area in the Betaloo Sub-basin of the Northern Territory, Australia. The Beetaloo Sub-basin (Williams 2019) is a southern component of the PalaeoProterozic to MesoProterozoic McArthur Basin that contains up to 9 km of sediments and volcanics (Ahmad *et al.* 2013). Large areas of the Beetaloo Sub-basin are unconformably overlain by the Cambrian Kalkarindji Suite of volcanics (formerly known as the Antrim Plateau Volcanics) mostly in the form of extensive basaltic sheets, and the Kalkarindji is in turn completely covered by weakly or non-magnetic Phanerozoic Carpenteria and Georgina Basin and younger sediments. There has been considerable investigation of the petroleum prospectivity of the Beetaloo Sub-basin with multiple wells drilled and over 9,000 km of two-dimensional reflection seismic lines (Williams 2019; Markov *et al.* 2021). There is also complete regional aeromagnetic coverage of the area by the Northern Territory Geological Survey. The study area is covered by the 2014 Dunmarra survey (P1268) flown on north–south flightlines at 400 m spacing and a nominal 80 m terrain clearance.

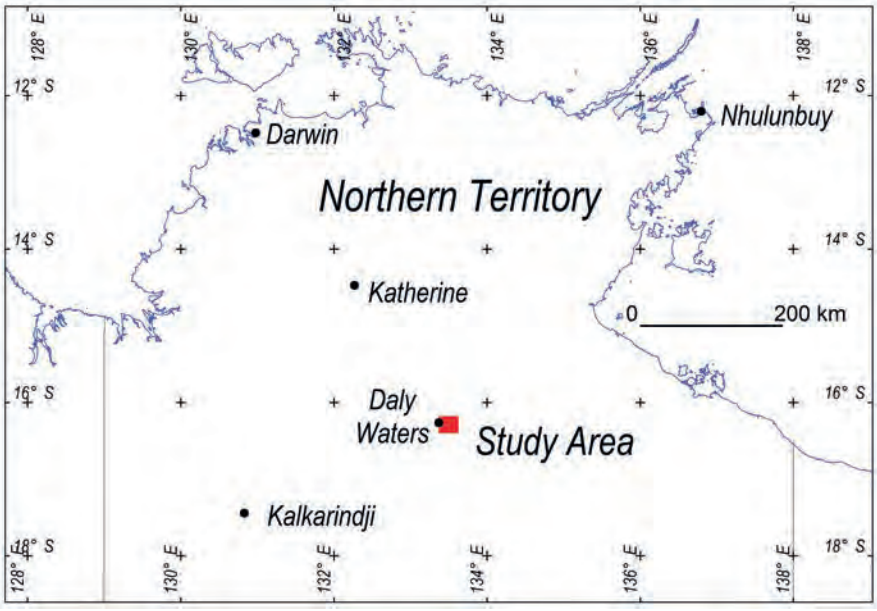

Fig. 12.3. Location of the study area over the Kalkarindji basalts in the Beetaloo Basin of the Northern Territory.

The TMI image in Fig. 12.4 shows contrast between the rough image texture of short-wavelength field variations due to shallow magnetisation contrasts across the top of the Kalkarindji basalts (covering much of the area in Fig. 12.4) and the smoother, longer-wavelength field variations over deeper magnetisation contrasts where the sheet is absent (the eastern section of Fig. 12.4). The highest amplitude magnetic field variations in Fig. 12.4 are over the sharp eastern edge of the sheet of Kalkarindji basalts. Consistent with magnetisation parallel to the southern hemisphere geomagnetic field, northern edges of the sheet have predominantly positive anomalies and southern edges have predominantly negative anomalies. This is illustrated in Fig. 12.5 that shows modelling of a grid traverse over a north-eastern tip of the sheet with the major field variations marking its edges. As shown in Fig. 12.5, the field variation can be well explained by a sub-horizontal sheet of

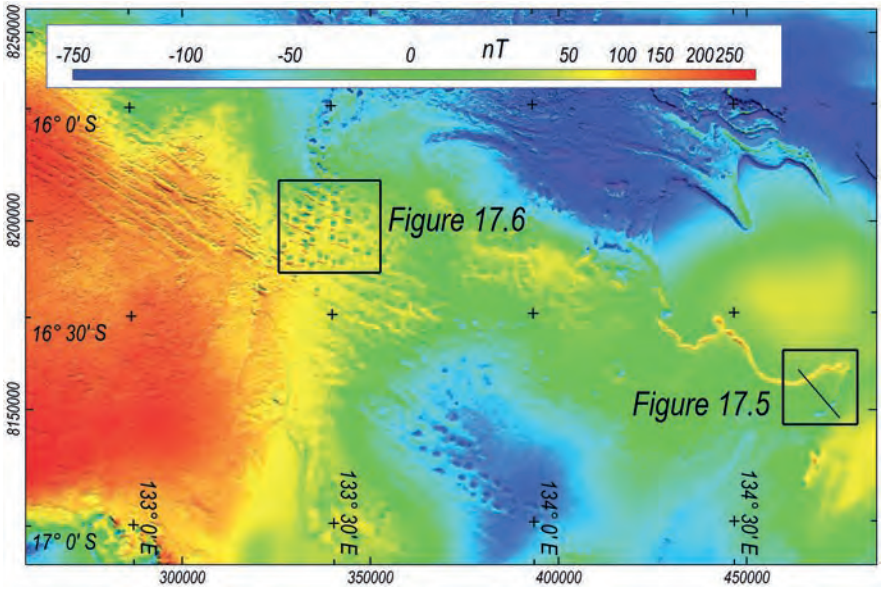

Fig. 12.4. TMI over the study area shown in Fig. 12.3.

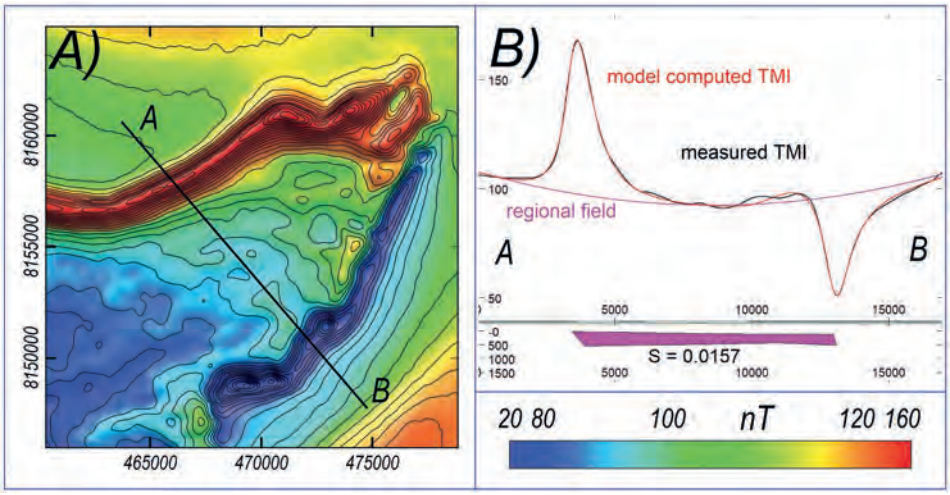

Fig. 12.5. A) TMI image and line of section over a north-east corner of the sheet of Kalkarindji basalts and B) a model along the line of section.

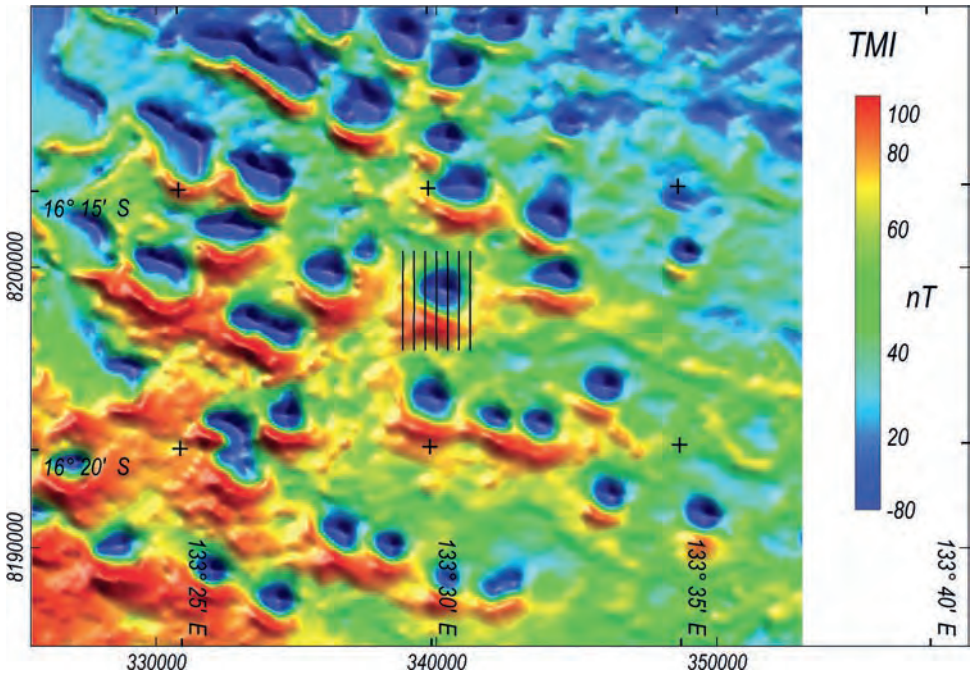

Fig. 12.6. TMI detail of the area located in Fig. 12.4. Modelling of the central anomaly marked by the north–south flightlines (400 m spacing) is shown in Fig. 12.7.

homogeneous magnetic susceptibility of between 0.01 and 0.02 SI and ~500 m thickness. There is little sensitivity to the specific thickness or magnetic susceptibility values of the best-fit model, that almost certainly represents a far more complex distribution of magnetisation (possibly including multiple layers). In modelling a single line of data there is also little sensitivity to magnetisation direction.

Over substantial areas of the Kalkarindji basalts (including the north-west area of Fig. 12.4) there are sharp local, parallel and equi-spaced linear magnetic field variations marking vertical displacements of the top of the sheet across steeply dipping faults that are imaged in the seismic sections (Markov *et al.* 2021). In the study area this pattern of magnetic field variation is mostly replaced by series of elliptic negative anomalies aligned in rows along the dominant east-south-east to west-north-west faulting direction. This pattern is only seen in areas that are clearly within the sub-crop of the Kalkarindji basalts and is interpreted as due to local

destruction of the magnetised sheet by hot fluids flowing along the intersections of fault and/or joint patterns that cut the sheet (Foss and Dhu 2016). This interpretation is supported by discovery of bitumen within and above the Kalkarindji volcanics (Glass *et al*. 2013) that may be hydrocarbons from a petroleum system in the underlying basin that were entrapped in the fluid flow. Detail of an area of these TMI anomalies (located in Fig. 12.4) is shown in Fig. 12.6. The anomalies are predominantly negative with a weaker positive to the south. Many are elongated parallel to the interpreted major faulting direction and most have peak to trough ranges of 100 to 200 nT.

If the area of Fig. 12.6 was underlain by a homogeneous smooth-topped horizontal sheet of Kalkarindji basalt with distant edges, the sheet would not have any obvious magnetic field expression. The pattern of the individual anomalies in Fig. 12.6 is consistent with magnetisations oppositely directed to the local geomagnetic field (reverse remanent magnetisations) but with knowledge of the magnetised Kalkarindji sheet they are interpreted as magnetisation contrasts due to absence of the normal magnetisation of the sheet. The section of north–south flightlines plotted in Fig. 12.6 highlight an anomaly that I have inverted using a polygonal-section body of horizontal top and bottom and free magnetisation direction (see Fig. 12.7). Inversion places the body at approximately the same depth and with approximately one-half of the depth-extent as the induced-magnetisation model of the sheet shown in Fig. 12.5 (neither of these parameters are well constrained). The contrast magnetisation of the model is 1.0 A/m with an inclination of +37°, declination 195°. On assumption that the body represents a hole of much lower magnetisation than the surrounding sheet, the sheet magnetisation can be inferred as ~1.0 A/m with an inclination of −37° and a declination of 15°. This direction is rotated by 12° from the local geomagnetic field, suggesting that there is some contribution from remanent magnetisation. The apparent magnetisation of the hole is approximately twice that of the apparent induced magnetisation of the sheet estimated in the model of Fig. 12.5. This gives the two models similar products of magnetisation and depth extent, consistent with the assumption that the reverse anomaly is due to a hole in the sheet filled with material of low intensity of magnetisation. Each of the inferred holes in the sheet provide an opportunity to estimate its local magnetisation. This is most conveniently achieved by inverting for the magnetisation contrasts of the holes and then assigning the reverse of those magnetisations to the sheet.

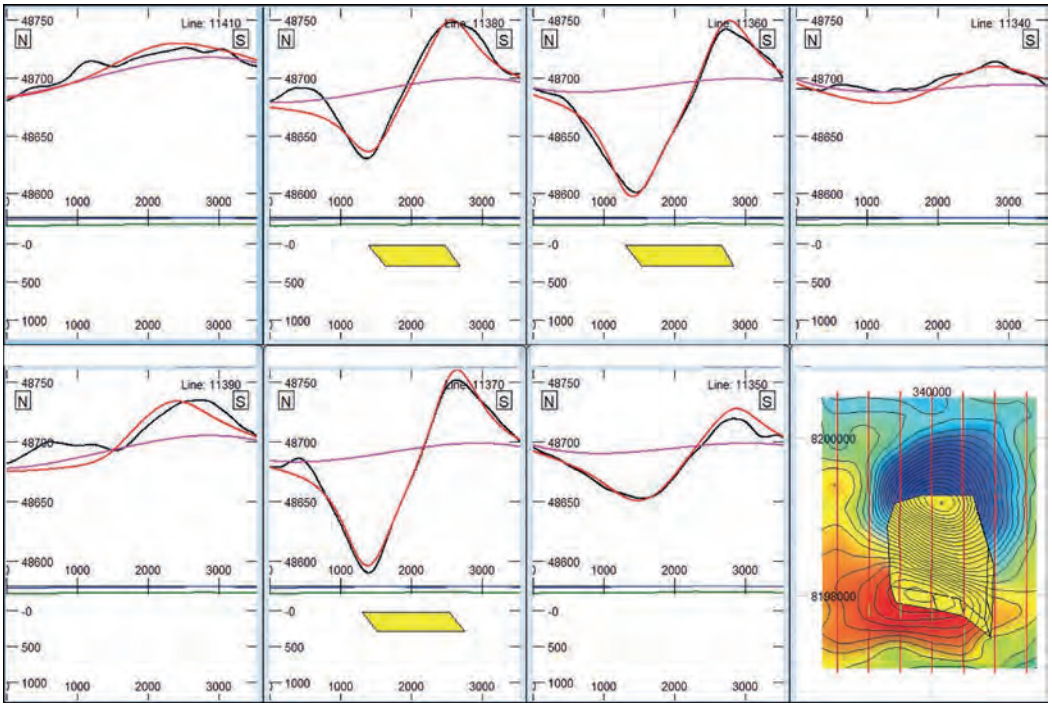

Fig. 12.7. Flightline sections through the model derived from inversion of the anomaly located in Fig. 12.6. The black traces are the measured field, magenta is the assigned background field and the red trace is the model-computed field.

12.3 A NEGATIVE MAGNETISATION CONTRAST ANOMALY OVER A PRESUMED BURIED GRANITE NORTH OF CEDUNA, SOUTH AUSTRALIA

To further illustrate recovery of estimates of magnetisation from anomalies that are the expression of negative magnetisation contrasts I present and extend a study by Foss *et al*. (2020) over a buried granite near Ceduna, South Australia in the southern Gawler Craton (Fig. 12.8). The TMI image in Fig. 12.9 is generated from data acquired on the 2014 South Australian PACE (Plan for Accelerating Exploration) Streaky Bay survey. The survey was flown on east–west flightlines at 200 m spacing and a nominal 60 m terrain clearance. Within the study area there is a range of almost 1,000 nT due to variable magnetisation of the southern Gawler Craton basement that underlies a thin cover of poorly consolidated Eucla Basin sediments. The basement rocks assigned to the Saint Peter Suite of the Nuyts Domain (Ferris and Fairclough 2007; Pawley *et al*. 2016; Reid *et al*. 2019) are undifferentiated within the study area because of the lack of outcrop and are mostly known from coastal exposures to the south. The rocks are dominantly granitic but with a range of inter-banded felsic to mafic and ultramafic rocks, interpreted to have been generated from magma mixing. The nearest basement outcrop, 10 km to the north-east, is assigned to the Hiltaba Granite as shown in the geological map by Blissett (1977) in Fig. 12.10.

The anomaly of interest in Fig. 12.9 is the broad magnetic low that has only minor internal field variation and a sharp, almost elliptic outline. The mostly simple shape of the anomaly, cross-cutting the complex magnetic field expressions of the surrounding basement suggests that the body may be a relatively late-stage intrusion of homogeneous, weak magnetisation as is commonly associated with late or post-orogenic granites. The magnetic low could be explained as due to a region of increased depth to the magnetised basement underlying an essentially non-magnetic cover, but the elliptic, smoothly curved sharp field change defining the edge of the anomaly is more consistent with a granite contact than with basement downthrow across faults that would be expected to consist of linear segments. Gravity variation coincident with the magnetic anomaly does not support confident interpretation because of the wide, 7 km spacing of the gravity stations, but the negative c. 100 μm/sec^2 gravity variation (based largely on a single station towards the centre of the magnetic anomaly) is also consistent with a granite emplaced into a more mafic, denser basement (Foss *et al*. 2020).

There are two major, broadly bifold classifications of granite as 'I-type' and 'S-type' (Chappell and White 1974) based on whole-rock geochemical and mineralogical inference of the igneous or sedimentary nature of the original melt zone, and of 'ilmenite series' and

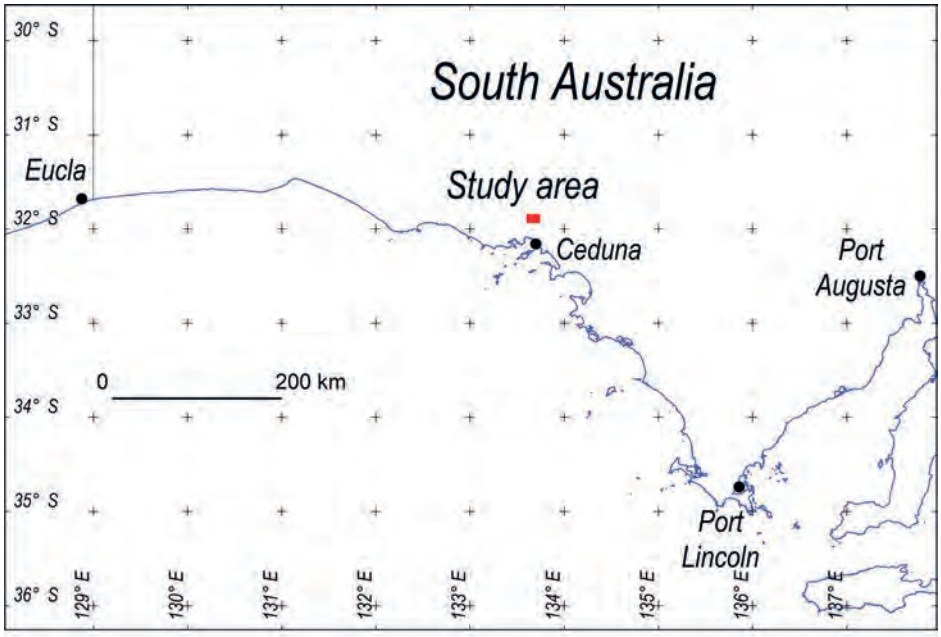

Fig. 12.8. Location of the study area near Ceduna in the southern Gawler Craton, South Australia.

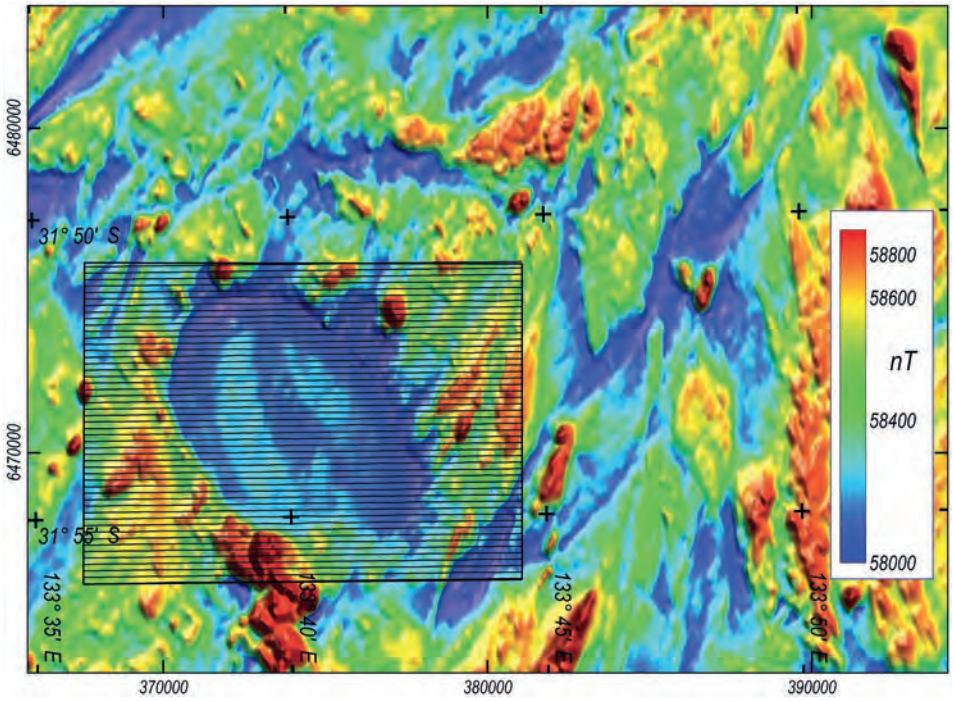

Fig. 12.9. Ceduna area TMI. The east–west flightlines show the area of the main inversion.

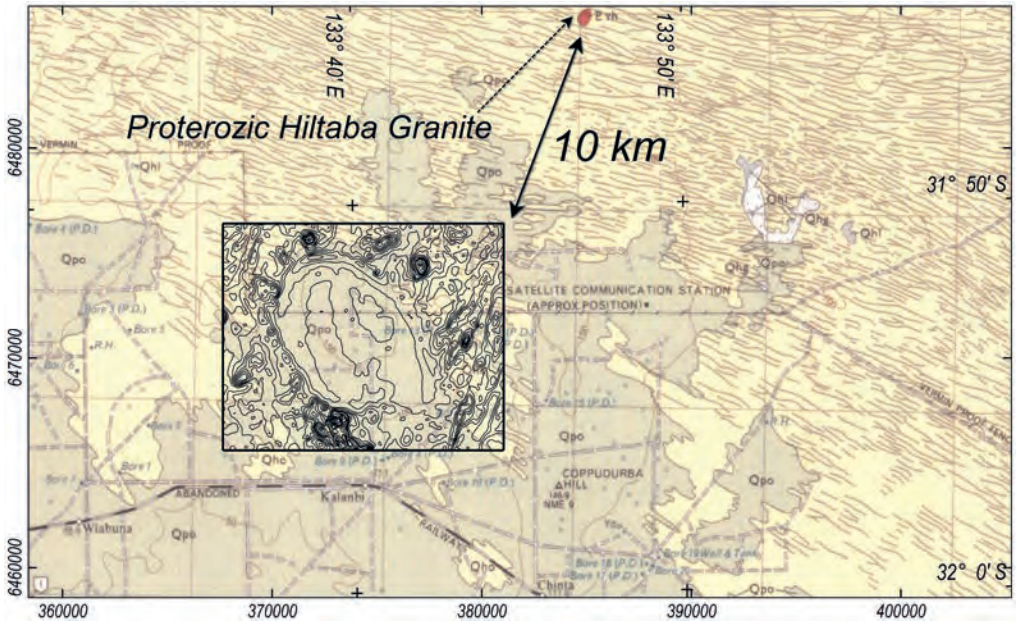

Fig. 12.10. Ceduna area 1:25,000 geology map (Blissett 1997) with TMI contours (100 nT interval). There is a single basement outcrop with the rest of the area covered by various Quaternary units.

'magnetite series' (Ishihara 1977) based on their minor iron and titanium oxide opaque minerals that ties directly to magnetisation. There is approximate correspondence between (generally) more strongly magnetised I-type and magnetite series granites and (generally) weakly magnetised S-type and ilmenite series granites.

In the southern Gawler Craton, samples of the Saint Peter Suite have variously been classified as I-type, S-type and A-type (anorogenic or anhydrous) (Frost *et al.* 2001) possibly because of complexities of magma mixing or because many of the granite samples are extensively altered.

In the study of the Kalkarindji volcanics the magnetisation contrast was against a sheet of apparently homogeneous magnetisation, but in this study the magnetic field variations are more complicated. Within and around the study area complex magnetic field variations include several small, relatively simple and isolated anomalies (Fig. 12.11) each defined on three to five east–west flightlines suitable for approximate determination of those local source magnetisation contrasts. These discrete anomalies highlighted in Fig. 12.11 have been independently inverted using plunging elliptic-section pipe homogeneous magnetisation models (Foss *et al*. 2020). Figure 12.12 shows measured and model-computed TMI for the anomaly located in Fig. 12.11 (anomaly 'L' in Foss *et al*. 2020). The complexity of this anomaly is not completely revealed by the 200 m flightline spacing, as is evident from the sharp

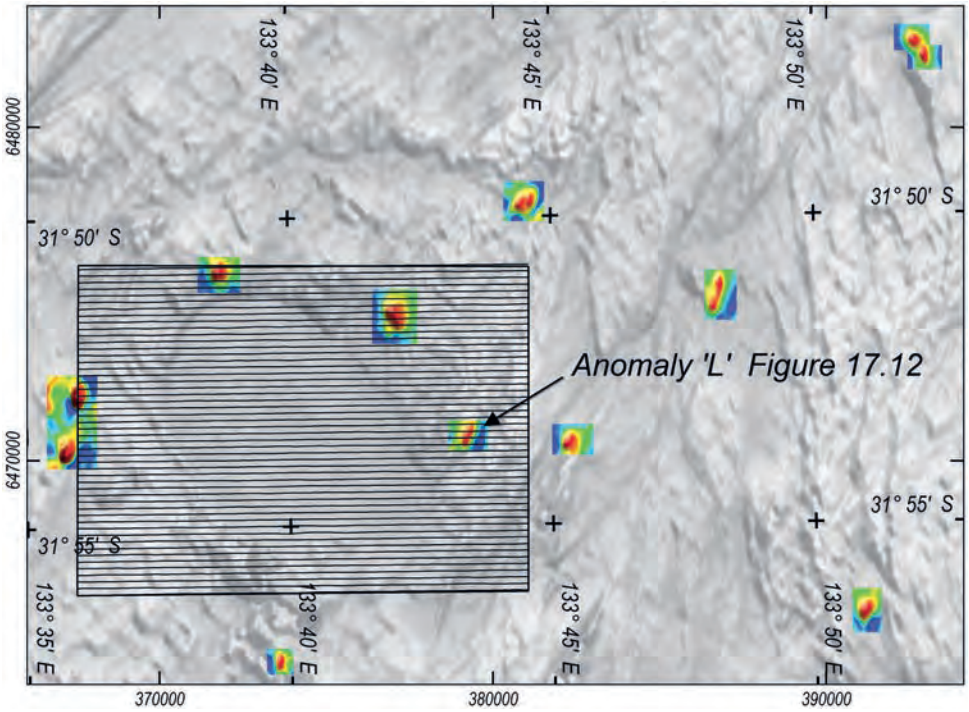

Fig. 12.11. Distribution of selected anomalies that have been individually inverted, shown over a grey-scale image of TMI. Most anomalies have a peak-to-trough range of 100 to 200 nT.

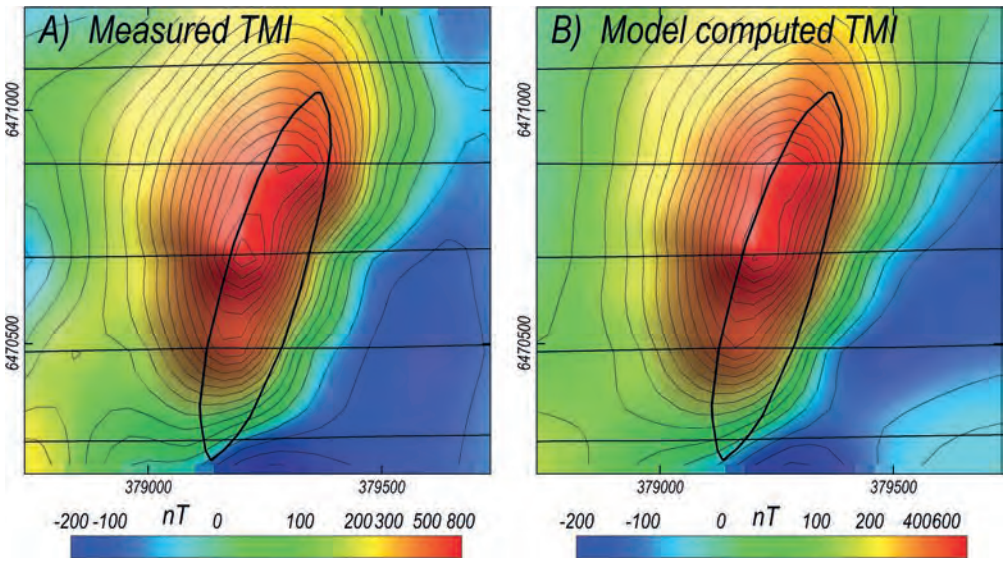

Fig. 12.12. A) measured and B) model-computed TMI over the anomaly located in Fig. 12.11.

differences in amplitude of the three adjacent flightlines across its centre. The model matches the field well on the available flightlines but may not well represent the (unknown) field between them. However, uncertainty of each inversion mostly arises from ambiguity in anomaly separation from complex background fields.

To study magnetisation contrasts between the granite and basement without edge effects from truncation of the models, I assigned magnetisation to the granite in the centre of the model and zero-magnetisation to the bounding basement, selecting 'standard' basement by excising sharp magnetic highs over interpreted strong intra-basement magnetisations (the image gaps in Fig. 12.13). Following the inversions I reassigned magnetisation by setting the standard basement magnetisation (that had been held at zero in the inversions) to the reverse of the granite body magnetisation and setting the granite body magnetisation to zero. A north–south range of 10 km for the model-computed field (50 flightlines at 200 m spacing) covers the variation of

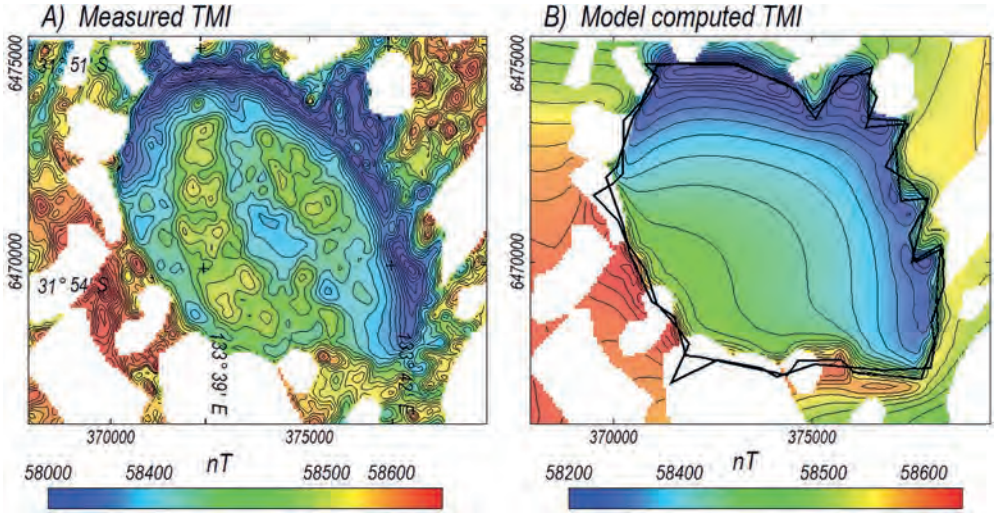

Fig. 12.13. A) measured TMI with high-amplitude basement anomalies excised and B) model-computed TMI (from inversion of even-numbered flightlines) with outline plans of the tops of the odd- and even-numbered inversion models.

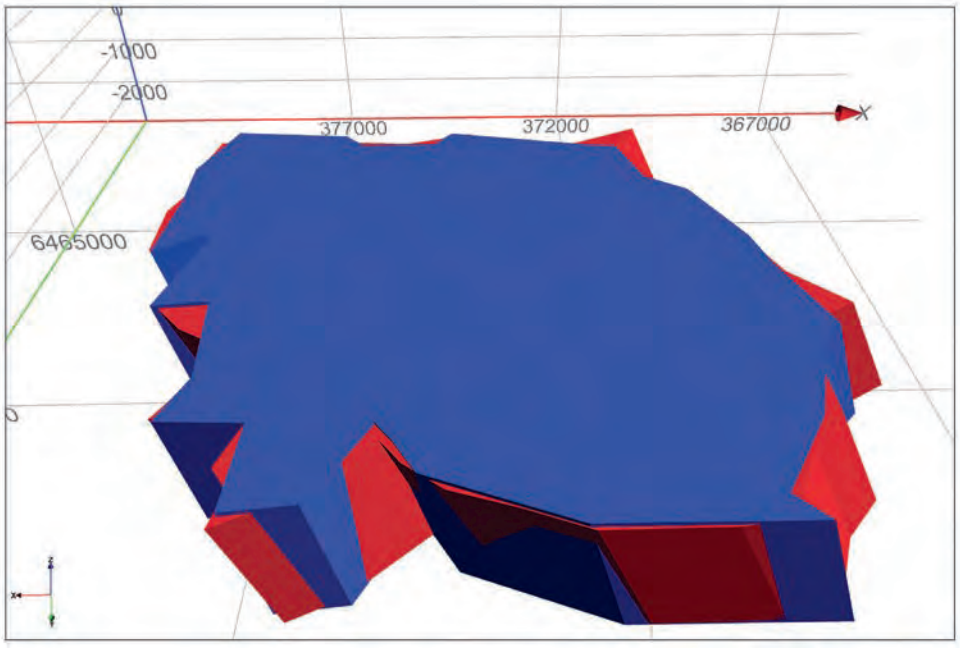

Fig. 12.14. Perspective of the granite inversion models: Blue from the odd-numbered and Red from the even-numbered flightlines.

interest (see Fig. 12.9). I split the flightlines into odd-numbered and even-numbered sets for independent inversion to investigate model repeatability. The study by Foss *et al*. (2020) first represented the granite body with elliptic-section horizontal topped and bottomed sheets, and after an approximate fit to the data had been achieved further inverted these bodies allowing independent movement of vertices defining their horizontal sections. In this study, I digitised the outline of a starting granite model from the TMI image and again used a staged inversion to first solve for the bulk properties of horizontal and vertical position, depth extent and magnetisation contrast. I then further inverted the bodies adding independent movement of the digitised vertices. To encourage stability, these inversions were performed in series of iterations, each allowing only short-distance movement of the vertices from their initial positions. In each iteration series the permitted ranges of the vertices were reset around their final positions in the previous series. Allowing larger single displacements of the vertices might help the models escape local data-misfit minima through exploration of a wider model space, but at the practical cost of a larger number of wasted computations and less effective search of the model space. Figure 12.13B shows the field computed from the odd-numbered line inversion model together with the outlines of the tops of the models from both the odd- and even-numbered line inversions. Comparison of the input data (Fig. 12.13A) and the field computed from an inversion model (Fig. 12.13B) shows that the inversions successfully explain the major long-wavelength features of the input data but lack the complexity to reproduce the short-wavelength features. The objective of inversion is not to match the input data (the task of its objective function) but to support speculation about the geology and magnetisation. These inversions clearly establish that key characteristics of the data are compatible with the model concept that the observed anomaly is due to a single homogeneous weak magnetisation surrounded by stronger magnetisation (also possibly homogeneous at broad scale after local anomalous magnetisations are excised).

Figure 12.14 shows a perspective view of the odd-line and even-line granite inversion model bodies (blue and red respectively) and statistics of the model magnetisations are reported in Table 12.1. The two bodies in Fig. 12.14 and the corresponding models of Foss *et al*. (2020) are all similar. The tops of three of the four model bodies are between 200 and 210 m below the mean ground level

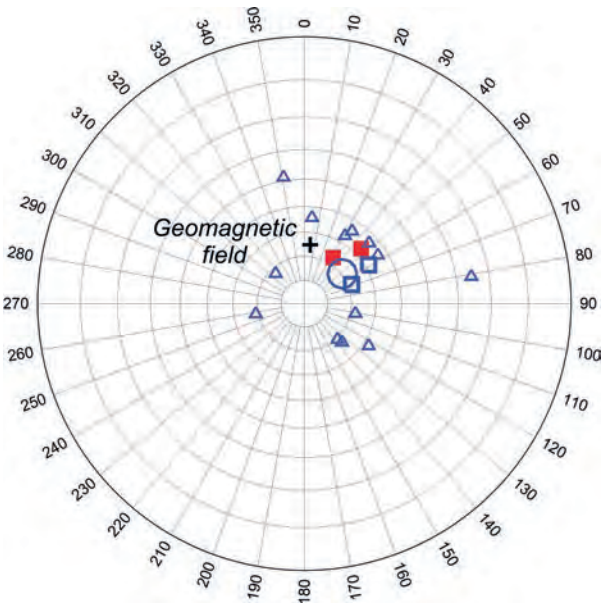

Fig. 12.15. Model magnetisation directions (all negative inclination): blue triangles – small anomalies, blue circle – small anomalies mean magnetisation, blue squares – basement estimates Foss et al. (2020), red squares – basement estimates this study.

(the fourth is 240 m). More reliable spot estimates of depth to magnetisation would best be recovered from single flightline inversions over the western and eastern edges of the body that are almost perpendicular to the flightlines (and on tie-line intersections with the northern and southern edges of the body). Estimated magnetisation contrasts for the four bodies are between 0.42 and 0.59 A/m (Table 12.1) and variations in depth extent are between 1,160 and 1,630 m, with considerable trade-off between the two parameters, such that the magnetic moments of the bodies are all between 32 and 35 $A.m^2.10^9$ as reported in Table 12.1 (the cross-sectional areas of the four granite model bodies are very similar).

Figure 12.15 shows magnetisation directions of the models. The 13 individual high-amplitude positive anomaly models have a range of estimated magnetisation directions, possibly as a combination of true variation in magnetisation direction and errors arising from incorrect anomaly separation (Foss *et al*. 2020). The $\alpha 95$ of the population is 14° (Foss *et al*. 2020) and the angular separation between the mean direction and the geomagnetic field is 18° (Table 12.1) suggesting that the magnetisations include a rotated remanent component. The two inversions by Foss *et al*. (2020) of the main granite anomaly gave a mean magnetisation estimate only 9° different to the mean of the positive anomaly

Table 12.1. Model magnetisation details (*after reversal of direction from the granite-body inversion model).

Study	Inversion	Volume (km3)	Magnetic moment (A.m2.109)	Magnetisation Intensity (A/m)	Dec-lination	Inc.-lination	ARRA
Foss et al. 2020	Mean of Thirteen anomalies			13.2	52°	–70°	18°
Foss et al. 2020	Odd-lines	77	32	0.422	68°*	–68°*	24°
Foss et al. 2020	Even-lines	75	33	0.440	59°*	–59°*	25°
this study	Odd-lines	62	32	0.520	32°*	–67°*	11°
this study	Even-lines	59	35	0.593	46°*	–57°*	21°

magnetisation directions, supporting an interpretation that the anomalous and 'standard' basement magnetisations are similar in direction and only differ in strength. The mean of the two granite-anomaly basement magnetisation estimates in this study is 11° different to the estimate by Foss *et al*. (2020) but is still only 10° from the mean of the positive anomaly directions, so the conclusion that these are the same direction is also supported by these inversion results.

The inversion models do not address magnetisation of the complex high-amplitude anomalies excised as shown in Fig. 12.13. It would be possible to restore that data and introduce additional model bodies to explain the anomalous magnetisations. However, those field variations were excluded because they were considered too complex to provide reliable inversion models. Addressing those anomalies in inversion of the complete dataset would result in a more complete representation of the magnetisation around the granite but would be unlikely to provide new insights into the geology or magnetisation. If those complex anomalies themselves are the focus of interest they could be inverted individually, but with necessarily lower reliability than inversion of the better-defined large granite anomaly.

12.4 CONCLUSIONS

With appropriate selection of the background field, the vector contrast between two magnetisations can be found by magnetic field modelling and inversion with either magnetisation set to zero. This includes the case of a weaker magnetisation enclosed within a stronger one (a magnetisation deficit anomaly). In the case that one magnetisation is much stronger but is set to zero in modelling or inversion, its value is the reverse (of equal strength and opposite direction) to the estimate obtained for the other magnetisation. Without constraints such as for magnetisations that form part of a terrain or bathymetric surface with contrast against a known zero magnetisation of air or water, it is not possible to derive either absolute magnetisation without knowing or assuming the other. Selection of which magnetisation to set to zero to obtain the contrast value can be decided by convenience – generally depending on the distribution of the magnetisations. In both the case of the holes in the Kalkarindji basalt sheet and of the buried granite near Ceduna it is more convenient to assign magnetisation to the included, more weakly or non-magnetised confined body and then reverse the vector to give the interpreted magnetisation of the surrounding material.

REFERENCES

Ahmad M, Dunster JN, Munson TJ (2013) 'Chapter 15: McArthur Basin': in Ahmad M and Munson TJ (compilers). Geology and mineral resources of the Northern Territory. Northern Territory Geological Survey, Special Publication 5.

Blissett AH (1977) 'Childara, Sheet SH/53–14, 1:250000 geological series'. Geological Survey of South Australia, Adelaide.

Chappell BW, White AJR (1974) Two contrasting granite types. *Pacific Geology* **8**, 173–174.

Ferris GM, Fairclough MC (2007) 'Explanatory Notes for the CHILDARA 1:250 000 Geological Map'. South Australia. Department of Primary Industries and Resources. Report Book 2007/8.

Foss CA, Dhu T (2016) The bark without a dog – magnetic anomalies over holes in a volcanic sheet in the greater McArthur Basin, NT. *ASEG Extended Abstracts* **2016**(1), 1–5. doi:10.1071/ASEG2016ab276

Foss CA, Gouthas G, Katona LF, Hutchens MF, Reed GD, Heath PJ (2020) 'Gawler Craton Airborne Geophysical Survey Region 5, Streaky Bay – Enhanced geophysical imagery and magnetic source depth models'. Report Book 2020/00020. Department for Energy and Mining, South Australia, Adelaide.

Frost RB, Barnes CG, Collins WJ, Arculus RJ, Ellis DJ, Frost CD (2001) A geochemical classification for granitic rocks. *Journal of Petrology* **42**, 2033–2048. doi:10.1093/petrology/42.11.2033

Glass LM, Ahmad M, Dunster JN (2013) 'Chapter 30: Kalkarindji Province': in Ahmad M and Munson TJ (compilers). 'Geology and mineral resources of the Northern Territory'. Northern Territory Geological Survey, Special Publication 5.

Ishihara S (1977) The Magnetite-series and Ilmenite-series Granitic Rocks. *Minería y Geología* **27**, 293–305.

Markov J, Foss CA, Swierczek E, Delle Piane C (2021) 'Kalkarindji through the structural lens: structural characteristics of the Kalkarindji basalt from non-seismic geophysical data'. AGES Proceedings, Northern Territory Geological Survey, pp. 43–47.

Pawley MJ, Reid AJ, Dutch RA (2016) Magmatic systems of the Paleoproterozoic St Peter Suite, Western Gawler Craton: insights from reconnaissance mapping. *Mesa Journal* **81**, 4–12.

Reid AJ, Pawley MJ, Wade C, Jagodzinski EA, Dutch RA, Armstrong R (2019) Resolving tectonic settings of ancient magmatic suites using structural, geochemical and isotopic constraints: the example of the St Peter Suite, southern Australia. *Australian Journal of Earth Sciences* **67**, 31–58. doi:10.1080/08120099.2019.1632224

Williams B (2019) 'Definition of the Beetaloo Sub-basin'. Northern Territory Geological Survey, Record 2019–015.